



HAL
open science

A companion in V1247 Ori supported by motion in the pattern of the spiral arm

Bin B. Ren, Chen Xie, Myriam Benisty, Ruobing Dong, Jaehan Bae, Tomas Stolker, Rob G. van Holstein, John H. Debes, Antonio Garufi, Christian Ginski, et al.

► **To cite this version:**

Bin B. Ren, Chen Xie, Myriam Benisty, Ruobing Dong, Jaehan Bae, et al.. A companion in V1247 Ori supported by motion in the pattern of the spiral arm. *Astronomy & Astrophysics*, 2024, 681, 10.1051/0004-6361/202348114 . insu-04479019

HAL Id: insu-04479019

<https://insu.hal.science/insu-04479019>

Submitted on 10 Mar 2024

HAL is a multi-disciplinary open access archive for the deposit and dissemination of scientific research documents, whether they are published or not. The documents may come from teaching and research institutions in France or abroad, or from public or private research centers.

L'archive ouverte pluridisciplinaire **HAL**, est destinée au dépôt et à la diffusion de documents scientifiques de niveau recherche, publiés ou non, émanant des établissements d'enseignement et de recherche français ou étrangers, des laboratoires publics ou privés.

LETTER TO THE EDITOR

A companion in V1247 Ori supported by motion in the pattern of the spiral arm^{★,★★}

Bin B. Ren^{1,2,★★} , Chen Xie^{3,4,★★} , Myriam Benisty^{1,2} , Ruobing Dong⁵ , Jaehan Bae⁶ , Tomas Stolker⁷ ,
Rob G. van Holstein⁸ , John H. Debes⁹ , Antonio Garufi¹⁰ , Christian Ginski¹¹ , and Stefan Kraus¹² 

¹ Université Côte d'Azur, Observatoire de la Côte d'Azur, CNRS, Laboratoire Lagrange, Bd de l'Observatoire, CS 34229, 06304 Nice Cedex 4, France

e-mail: bin.ren@oca.eu

² Université Grenoble Alpes, CNRS, Institut de Planétologie et d'Astrophysique (IPAG), 38000 Grenoble, France

³ Department of Physics and Astronomy, The Johns Hopkins University, 3701 San Martin Drive, Baltimore, MD 21218, USA

⁴ Aix Marseille Univ., CNRS, CNES, LAM, Marseille, France

e-mail: chen.xie@lam.fr

⁵ Department of Physics & Astronomy, University of Victoria, Victoria, BC V8P 5C2, Canada

⁶ Department of Astronomy, University of Florida, Gainesville, FL 32611, USA

⁷ Leiden Observatory, Leiden University, Niels Bohrweg 2, 2333 CA Leiden, The Netherlands

⁸ European Southern Observatory, Alonso de Córdova 3107, Vitacura Casilla 19001, Santiago, Chile

⁹ AURA, for ESA, Space Telescope Science Institute, 3700 San Martin Dr., Baltimore, MD 21218, USA

¹⁰ INAF, Osservatorio Astrofisico di Arcetri, Largo Enrico Fermi 5, 50125 Firenze, Italy

¹¹ School of Natural Sciences, University of Galway, University Road, H91 TK33 Galway, UK

¹² Astrophysics Group, Department of Physics & Astronomy, University of Exeter, Stocker Road, Exeter EX4 4QL, UK

Received 29 September 2023 / Accepted 6 December 2023

ABSTRACT

While nearly two dozen spiral arms have been detected from planet-forming disks in near-infrared scattered light, none of their substellar drivers has been confirmed. By observing spiral systems in at least two epochs spanning multiple years and measuring the motion of the spirals, we can distinguish what causes the spirals and locate the orbits of the driving planets if the spirals are triggered by them. Upon a recent validation of this approach using the comotion between a stellar companion and a spiral, we obtained a second-epoch observation for the spiral system in the disk of V1247 Ori in the *H*-band polarized scattered light using Very Large Telescope (VLT), SPHERE, and IRDIS. By combining our observations with archival IRDIS data, we established a 4.8 yr timeline to constrain the spiral motion of V1247 Ori. We obtained a pattern speed of $0^{\circ}.40 \pm 0^{\circ}.10 \text{ yr}^{-1}$ for the northeast spiral. This corresponds to an orbital period of $900 \pm 220 \text{ yr}$, and the semimajor axis of the hidden planetary driver therefore is $118 \pm 20 \text{ au}$ for a $2.0 \pm 0.1 M_{\odot}$ central star. The location agrees with the gap in ALMA dust-continuum observations, which provides joint support for the hypothesis that a companion drives the scattered-light spirals while carving a millimeter gap. With an angular separation of $0^{\prime}.29 \pm 0^{\prime}.05$, this hidden companion is an ideal target for JWST imaging.

Key words. techniques: high angular resolution – protoplanetary disks – planet-disk interactions – stars: individual: V1247 Ori

1. Introduction

Over the course of the past decade of direct-imaging attempts for self-luminous planets using dedicated high-contrast imaging instruments (e.g., [Nielsen et al. 2020](#); [Vigan et al. 2021](#)), only a handful of these planets have newly been discovered and confirmed (e.g., [Macintosh et al. 2015](#); [Chauvin et al. 2017](#); [Keppler et al. 2018](#); [Haffert et al. 2019](#)). The low detection rate called for optimized and targeted observing strategies in more recent studies that included young systems (e.g., [Bohn et al.](#)

[2021](#)), stellar radial velocity (e.g., [Lagrange et al. 2019](#); [Nowak et al. 2020](#)), astrometric acceleration (e.g., [Currie et al. 2023](#); [Franson et al. 2023](#); [De Rosa et al. 2023](#); [Mesa et al. 2023](#)) evidence, and the morphological deviation of circumstellar disks (e.g., [Bae et al. 2019](#); [Haffert et al. 2019](#); [Wang et al. 2020](#)).

Targeted imaging based on deviations from stellar signals (e.g., radial velocity or astrometry) have produced fruitful results. It may take up to several decades to investigate whether planets exist by monitoring these signals (e.g., [Lagrange et al. 2019](#); [Currie et al. 2023](#)), however, and the monitoring relies on instruments whose stability and sensitivity could have improved significantly over time. Meanwhile, substructures engraved on circumstellar disks by planets have suggested that planets might exist (e.g., [Dong et al. 2015a, 2016a](#); [Bae et al. 2016](#); [Zhang et al. 2018](#); [Long et al. 2022](#)). Of all planet-induced structures, spiral arms might be the best systems for a targeted high-contrast imaging search because their planetary drivers

* Data files associated to Fig. 1 are available at the CDS via anonymous ftp to cdsarc.cds.unistra.fr (130.79.128.5) or via <https://cdsarc.cds.unistra.fr/viz-bin/cat/J/A+A/681/L2>

** Based on observations performed with VLT/SPHERE under program ID 0102.C-0778 and 111.24GG.

*** Marie Skłodowska-Curie fellow.

tend to be more massive (e.g., Bae et al. 2018) and thus more luminous (e.g., Spiegel & Burrows 2012). They are more likely to be accessed by the current generation of high-contrast imaging instruments.

The pattern motion of a spiral arm when driven by a companion follows the orbital motion of its driver (e.g., Dong et al. 2015a; Bae & Zhu 2018). By tracing the motion of the spirals, we can constrain the orbit of a hidden driver (Ren et al. 2018) and trace the motion back to its cause. In this way, we can determine the mechanism (i.e., companion-driven and gravity-instability-induction: Ren et al. 2020). By showing the first dynamic evidence of comotion between a stellar companion and a spiral in the system HD 100453, Xie et al. (2023) confirmed the theory of companion-driven spirals (e.g., Dong et al. 2015a, 2016a; Bae et al. 2016). This confirms that the monitoring of spiral motion is a major science case for future extremely large telescopes (Maire et al. 2021). After first light for the current high-contrast imagers in ≈ 2015 , we can now reimage the spirals with the same instrument across a separation of ≈ 5 yr (e.g., Ren et al. 2020; Xie et al. 2023), and we therefore expect a rapid expansion of these studies (Benisty et al. 2023). When a spiral system is confirmed to be driven by hidden planetary companions, we can conduct targeted imaging to determine whether a planet exists (e.g., Wagner et al. 2019, 2023; Boccaletti et al. 2021).

The known spiral arm hosts (e.g., Dong et al. 2018; Shuai et al. 2022), V1247 Ori include an A5III or F0V star (e.g., Kharchenko 2001; Vieira et al. 2003) located at 401 ± 3 pc (Gaia Collaboration 2023). With an estimated age of 7.0 ± 0.3 Myr (Garufi et al. 2018), it hosts a pair of nearly symmetric spiral arms in scattered light (e.g., *H*-band: Shuai et al. 2022) and a gap in Atacama Large Millimeter Array (ALMA) submillimeter/millimeter observations (e.g., Band 7: Kraus et al. 2017). Based on the morphology of the dust continuum, Kraus et al. (2017) proposed that a planet at ≈ 0.3 , or 120 au with the updated distances from *Gaia* DR3, from the star could carve the ALMA gap. While it is possible that the V1247 Ori spirals could be triggered by a recent stellar flyby (i.e., $\approx 10^4$ yr in time, and at a separation of about ten times the disk radius), using the location and proper motion measurements from *Gaia* DR3, Shuai et al. (2022) identified no flyby events for V1247 Ori. In addition, the spirals might be triggered by gravitational instability, but the disk-to-star mass ratio should be $q \gtrsim 0.25$ in Dong et al. (2015b), which contradicts the $q \approx 0.04$ from Yu et al. (2019). This combined evidence means that the system V1247 Ori might host a planetary companion that drives the spirals in scattered light. By reimaging V1247 Ori in scattered light at another epoch, we will be able to test observationally whether the spiral motion is consistent with being driven by a planet in the ALMA dust continuum gap.

To observationally constrain the motion pattern for existing spiral systems, the dedicated survey Spiral Arm Formation from mOtion aNalysis (SAFFRON; ESO programs 111.24GG and 112.25B7) acquires additional epoch(s) of existing spirals with a total allocation of 54.5 h from VLT, SPHERE, and IRDIS. For these systems, we can use the spiral motion to distinguish whether the motion is driven by a companion or by gravitational instability (Ren et al. 2020), predict the orbits of hidden drivers (e.g., Ren et al. 2018; Xie et al. 2021), and confirm the connection between known companion(s) and spiral(s) (Xie et al. 2023). Through SAFFRON observations, we aim to constrain the pattern motion for all the spiral systems in near-infrared scattered light (e.g., Shuai et al. 2022). Moreover, if the motions are consistent with being driven by companions, we will be able

to map the orbital distribution of these hidden planets. In this Letter, we report the first result from the SAFFRON survey for V1247 Ori.

2. Observation and data reduction

Using VLT, we observed V1247 Ori using the infrared dual-band imager and spectrograph (IRDIS; Dohlen et al. 2008) on SPHERE (Beuzit et al. 2019) in dual-beam polarimetric imaging (DPI; de Boer et al. 2020; van Holstein et al. 2020) mode at the *H* band ($1.625 \mu\text{m}$) on UT 2023 September 20 under ESO program 111.24GG in SAFFRON (PI: B. Ren). The observation complements the observation on 2018 November 16 under ESO program 0102.C-0778 (PI: S. Kraus) to enable a precise measurement of the motion of the spiral pattern.

To ensure that the motion of the spiral pattern was measured with similar data quality for the measurement of the spiral pattern motion, we minimized the observational difference as follows. Specifically, we adopted the same 32 s exposure in each integration. There are 9 polarimetric cycles through Q^+ , Q^- , U^+ , and U^- with three integrations per exposure in 2018 and 15 polarimetric cycles with one integration per exposure in 2023. We totaled 3456 s on-target time in 2018 and 1920 s in 2023. At the end of the observations, 128 s and 32 s total exposure were available for sky background removal in 2018 and 2023, respectively.

We reduced the two observed IRDIS DPI data sets using the IRDAP pipeline (van Holstein et al. 2017, 2020). In the reduction, we also adopted the parallactic angles calculated using the Stolker et al. (2019) pipeline for SPHERE. To enable precise measurement of the spiral location and motion in the further analysis, we additionally stretched the preprocessed cubes by 1.006 along the column direction of the detector to correct for the anamorphism from optical distortions in SPHERE (e.g., Schmid et al. 2018). Of the postprocessed data products from IRDAP, we used the star-polarization-subtracted local Stokes Q_ϕ map, which traces the distribution of dust particles on the surfaces of disks (e.g., Monnier et al. 2019), for the analysis. We present the Q_ϕ images from the two epochs and annotate the spiral arms in Fig. 1.

To reduce the impact of stellar light illumination as a function of stellocentric radius (the incident flux reduces as distance squared), the surface density distribution images were used to analyze the motion (e.g., Xie et al. 2023). Specifically, we scaled the surface brightness distribution for the two Q_ϕ images of V1247 Ori. We adopted an inclination of $30^\circ 0 \pm 1^\circ 0$ from face-on, and a position angle of $-64^\circ 6 \pm 0^\circ 4$ for the major axis of the disk from north to east from the ALMA analysis (Kraus et al. 2017). To correct for disk-flaring effects, we assumed that the disk scale height, h , follows $h/r = 0.05$, where r is radial separation (Kraus et al. 2017). We then computed the midplane stellocentric distances, r , for all image pixels, and multiplied the value at each pixel by r^2 to reveal the distribution of the scatterers, which typically trace the surface morphology and roughly trace the dust surface density.

3. Analysis

To measure the location of the spiral, we analyzed the r^2 -scaled Q_ϕ images as follows. First, we deprojected the disk images to face-on views. Second, we determined the local maxima of the spiral arm in polar coordinates: We performed three Gaussian profile fits with an additional constant in a total of ten free parameters (e.g., Ren et al. 2020; Xie et al. 2023). The additional

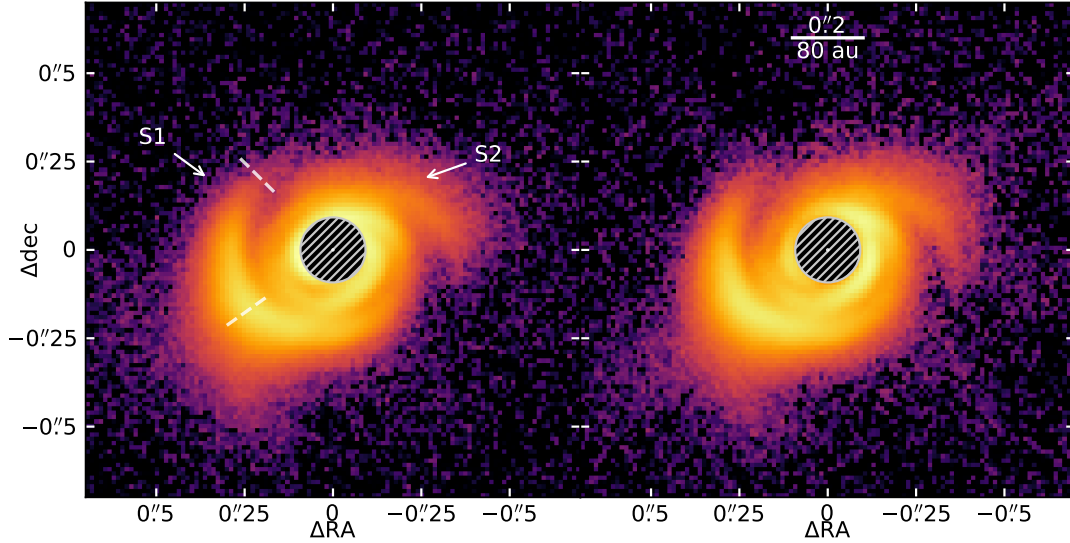


Fig. 1. Two epoch Q_0 images of V1247 Ori with SPHERE/IRDIS in H band on 2018 November 16 (left) and on 2023 September 20 (right). The color bars are in log scale. The dashed lines are the boundaries for the motion measurement in Fig. 2. (The data used to create this figure are available at the CDS.)

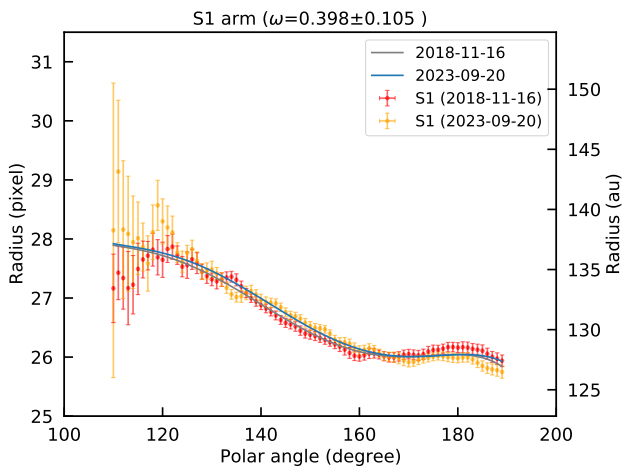


Fig. 2. Peak locations of spiral arm S1 between 110° and 190° in polar coordinates in the disk plane. The solid curves represent the best-fit model spiral for the peak locations (dots) between 2018 and 2023 ($t = 4.84$ yr), assuming the companion-driven scenario. The derived angular velocity of the motion of the spiral pattern is $0:40 \pm 0:10 \text{ yr}^{-1}$ counterclockwise.

constant takes the overall disk brightness offset at a specific location into account. Specifically, multiple spirals might exist at a specific azimuthal angle, and we therefore adopted three Gaussian profiles for the two wrapped arm components along the radial direction (e.g., the ≈ 2 o'clock region in Fig. 1). Third, in each azimuthal angle, we performed fittings to obtain the locations of the spiral arms with an angular step of 1° . We present the locations for a selected region of the northeast spiral S1 in Fig. 2. For measurements of the entirety of the two spirals, see Figs. A.1 and A.2. However, because the two spirals are visually merged interior to ≈ 125 au due to the finite resolution of VLT/SPHERE, the motion measurements for the entirety of the two spirals are likely biased. We therefore only focus on the exterior region of S1 marked in Fig. 1 in this study.

To simultaneously derive the spiral pattern motion and its morphological parameters, we fit p -degree polynomials with a

dummy variable to a given spiral arm in two epochs as described in Ren et al. (2020). The Schwarz information criterion, which penalizes the excessive use of parameters, is minimized at $p = 5$, and thus, we adopted the corresponding results for the motion analysis. Using the dummy variable, we simultaneously fit an identical but offset polynomial to a spiral at both epochs. The large extent of spiral arm S1 enables us to explore motion measurements for different parts of the spiral (see Fig. 2 for a specific area of S1, and Fig. A.1 for the entirety of S1).

The measurement of the location of the spiral and the pattern speed can be affected by multiple factors for V1247 Ori. On the one hand, with an inclination of $\approx 30^\circ$ (e.g., Kraus et al. 2017; Bohn et al. 2022), the spiral morphology of V1247 Ori might be distorted (limiting inclination of $\approx 20^\circ$: Dong et al. 2016b). On the other hand, global shadowing effects are visible in the northeast regions in Fig. 1, which might be cast by inner disks (e.g., Debes et al. 2017, 2023). Due to the non-negligible inclination of the system ($\approx 30^\circ$) and the given angular resolution of SPHERE (51 mas in H band for an effective pupil of 8.0 m), the location and motion measurement for the entirety of S1 and S2 in Figs. A.1 and A.2 might therefore be biased. Specifically, the morphology of the spiral can be altered when the disk is not seen face-on ($\geq 20^\circ$ inclination: Dong et al. 2016b), and when spirals are driven by an identical but eccentric companion (e.g., Calcino et al. 2020), Xie et al. (2023) showed that spirals might have different apparent motion.

To quantify the spiral motion, we focus on a specific region in the S1 spiral in Fig. 2 to measure the motion. As reported in Xie et al. (2023), the spiral location and motion should be measured for a disk surface that is approximately face-on through a combination of disk inclination and disk flaring. For this purpose, we focused on a spiral region in S1 with a stellocentric radius of 125–140 au, which spans an azimuthal coverage of $\approx 80^\circ$ from the disk midplane. In this region, the inclination and flaring of the spiral cause the disk surface to be closer to a face-on view, and we measured its spiral motion of S1 to be¹

$$\omega = 0:40 \pm 0:10 \text{ yr}^{-1}, \quad (1)$$

¹ The derived uncertainties presented in this Letter are 1σ unless otherwise specified.

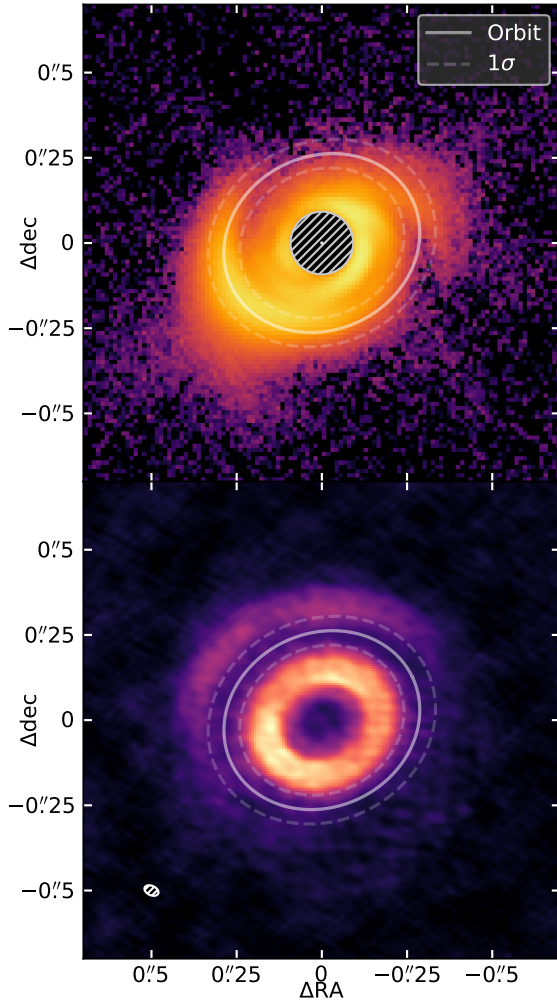


Fig. 3. Driver orbit from the motion of the S1 spiral pattern, overlaid on observations in the SPHERE H band Q_ϕ (top; UT 2023 September 20) and ALMA Band 7 continuum (bottom; UT 2017 August 9). For a central star with $2.0 \pm 0.1 M_\odot$, the $0^\circ:40 \pm 0^\circ:10 \text{ yr}^{-1}$ counterclockwise motion of the S1 spiral corresponds to a driver at $118 \pm 20 \text{ au}$, or $0^\circ:29 \pm 0^\circ:05$. Subject to motion measurement uncertainties here, the derived orbit is consistent with the $\approx 120 \text{ au}$ ALMA gap-opener proposed in Kraus et al. (2017) within 1σ .

counterclockwise in Fig. 2. We obtained the uncertainty in Eq. (1) using $\sigma = \sqrt{(\sigma_{\text{fit}})^2 + 2\sigma_{\text{north}}^2 + 2\sigma_{\text{centering}}^2} t^{-1}$, where σ_{fit} and σ_{north} are the uncertainties caused by the measurement of the spiral locations and the true north uncertainty of SPHERE, respectively. The time span between the two epochs is represented by t , which is 4.84 yr. The selected locations in S1 return a fitting uncertainty $\sigma_{\text{fit}} = 0^\circ:091 \text{ yr}^{-1}$. We adopted the true north uncertainty of SPHERE as $\sigma_{\text{north}} = 0^\circ:08$ in all epochs (Maire et al. 2016). We also adopted an astrometric uncertainty of $\approx 2 \text{ mas}$ (Zurlo et al. 2014, Fig. 7 therein), or 0.16 IRDIS pixel, and thus an offset of $\sigma_{\text{centering}} = 0^\circ:16$ in polar coordinates. The combined uncertainty in the motion rate is thus $\sigma = 0^\circ:10 \text{ yr}^{-1}$.

Data sampling and disk parameters may affect the measurement of the spiral motion. Different data sampling (e.g., a Nyquist sampling has an angular step of 5°) gives a consistent spiral motion of $0^\circ:46 \pm 0^\circ:18 \text{ yr}^{-1}$ with a slightly larger total uncertainty. Correlated noise in the oversampling case (an angular step of 1°) may lead to an underestimated total uncertainty. However, given the consistent motion measurements and the

minor impact on the uncertainty, a proper estimation of the correlated noise (e.g., Czekala et al. 2015) in the oversampling case is beyond the scope of this work. The impact from the disk parameters (e.g., inclination, flaring, and position angle) has been extensively analyzed (e.g., Sect. 4.5 of Ren et al. 2020, Sect. 4.2 of Xie et al. 2021, and Appendix D of Xie et al. 2023), showing that the corresponding impact resides within the derived motion uncertainty.

The pattern motion of S1 in the selected region in Fig. 1 is $\omega = 0^\circ:40 \pm 0^\circ:10 \text{ yr}^{-1}$ in Eq. (1), which corresponds to a driver at $118 \pm 20 \text{ au}$ on a circular orbit from a central star with $2.0 \pm 0.1 M_\odot$ (Garufi et al. 2018). To illustrate its orbit, we obtained the ALMA Band 7 continuum observations of V1247 Ori from Kraus et al. (2017). Together with the scattered-light Q_ϕ image, we present the predicted driver orbit in Fig. 3.

Our measurement in Fig. 2 cannot confidently rule out local gravitational motion, with a local Keplerian motion at 125 au ($0^\circ:3$) to 140 au ($0^\circ:35$) of $0^\circ:349 \text{ yr}^{-1}$ to $0^\circ:296 \text{ yr}^{-1}$, respectively. However, the disk-to-star mass ratio of V1247 Ori is $q \approx 0.04$ from Yu et al. (2019), which means that it is unlikely to trigger local gravitational instability for the spiral motion. If the V1247 Ori spirals were triggered by gravitational instability, the disk-to-star mass ratio should be $q \gtrsim 0.25$ in Dong et al. (2015b), which is more massive by about six times than the current ratio and is thus unlikely.

In comparison with the ALMA data, if the proposed gap-opening planet in Kraus et al. (2017) drives the spiral, the pattern motion of the spiral for a star with a mass of $2.0 \pm 0.1 M_\odot$ should be $0^\circ:39 \pm 0^\circ:01 \text{ yr}^{-1}$. This is consistent within 1σ with the measured pattern motion in Eq. (1). With our motion measurement, we offer dynamical evidence that a spiral-arm-driving planet probably exists in scattered light, and this driver simultaneously carves the millimeter gap in Kraus et al. (2017).

4. Conclusion

The pattern motion of spirals can inform us about their formation mechanisms (e.g., Ren et al. 2020). If it is driven by a companion, then the motion of the spiral pattern traces the orbit of its driver (e.g., Ren et al. 2018; Safonov et al. 2022). With two epochs of polarized-light observations spanning 4.84 yr, we constrained the pattern motion for the S1 spiral in scattered light in the V1247 Ori system to be $0^\circ:40 \pm 0^\circ:10 \text{ yr}^{-1}$ counterclockwise. For a $2.0 \pm 0.1 M_\odot$ star, this translates into a semi-major axis of $118 \pm 20 \text{ au}$, or $0^\circ:29 \pm 0^\circ:05$, for the hidden companion that drives the spiral arm.

The companion that drives the spiral arm in Fig. 3 is not yet imaged for V1247 Ori in ground-based observatories (e.g., Ohta et al. 2016; Willson et al. 2019; Follette et al. 2023; Wallack et al. 2023). Based on the misalignments between the inner and outer disks (e.g., Bohn et al. 2022; Wölfer et al. 2023), we can rule out such a companion-spiral connection at the $>5\sigma$ level from our motion measurements even if an inner companion exists that creates the inner cavity in ALMA and drives the spirals behind the coronagraph ($\approx 0^\circ:1$) in Fig. 1.

This hidden companion that might drive spiral(s) in scattered light and might carve a gap in the millimeter continuum is the first for which two different pieces of observational evidence have been presented that support its existence. Because ground-based instruments are limited in sensitivity for this driver (≈ 80 Jupiter mass; Ren et al. 2023) and because the JWST/NIRCam coronagraphic mode was demonstrated to have a superior sensitivity in Carter et al. (2023), and also because planetary drivers for a pair of symmetric spirals should have

5–10 Jupiter mass (i.e., Dong et al. 2015a; Bae et al. 2016), the driver we located here for V1247 Ori is an ideal target for coronagraphic imaging with the JWST/NIRCam.

Acknowledgements. We thank the anonymous referee for their comments and suggestions that improved the quality of this Letter. We thank Andrew Winter and Jochen Stadler for discussions. Based on observations collected at the European Organisation for Astronomical Research in the Southern Hemisphere under ESO programmes 0102.C-0778 and 111.24GG. This project has received funding from the European Union’s Horizon Europe research and innovation programme under the Marie Skłodowska-Curie grant agreement No. 101103114. This project has received funding from the European Research Council (ERC) under the European Union’s Horizon 2020 research and innovation programme (PROTOPLANETS, grant agreement No. 101002188). R.D. acknowledges financial support provided by the Natural Sciences and Engineering Research Council of Canada through a Discovery Grant, as well as the Alfred P. Sloan Foundation through a Sloan Research Fellowship. This Letter makes use of the following ALMA data: ADS/JAO.ALMA#2015.1.00986.S. ALMA is a partnership of ESO (representing its member states), NSF (USA) and NINS (Japan), together with NRC (Canada), MOST and ASIAA (Taiwan, ROC), and KASI (Republic of Korea), in cooperation with the Republic of Chile. The Joint ALMA Observatory is operated by ESO, AUI/NRAO and NAOJ. This work has made use of data from the European Space Agency (ESA) mission *Gaia* (<https://www.cosmos.esa.int/gaia>), processed by the *Gaia* Data Processing and Analysis Consortium (DPAC, <https://www.cosmos.esa.int/web/gaia/dpac/consortium>).

References

- Bae, J., & Zhu, Z. 2018, *ApJ*, 859, 119
 Bae, J., Zhu, Z., & Hartmann, L. 2016, *ApJ*, 819, 134
 Bae, J., Pinilla, P., & Birnstiel, T. 2018, *ApJ*, 864, L26
 Bae, J., Zhu, Z., Baruteau, C., et al. 2019, *ApJ*, 884, L41
 Benisty, M., Dominik, C., Follette, K., et al. 2023, *ASP Conf. Ser.*, 534, 605
 Beuzit, J. L., Vigan, A., Mouillet, D., et al. 2019, *A&A*, 631, A155
 Boccaletti, A., Pantin, E., Ménard, F., et al. 2021, *A&A*, 652, L8
 Bohn, A. J., Ginski, C., Kenworthy, M. A., et al. 2021, *A&A*, 648, A73
 Bohn, A. J., Benisty, M., Perraut, K., et al. 2022, *A&A*, 658, A183
 Calcino, J., Christiaens, V., Price, D. J., et al. 2020, *MNRAS*, 498, 639
 Carter, A. L., Hinkley, S., Kammerer, J., et al. 2023, *ApJ*, 951, L20
 Chauvin, G., Desidera, S., Lagrange, A. M., et al. 2017, *A&A*, 605, L9
 Currie, T., Brandt, G. M., Brandt, T. D., et al. 2023, *Science*, 380, 198
 Czekala, I., Andrews, S. M., Mandel, K. S., et al. 2015, *ApJ*, 812, 128
 de Boer, J., Langlois, M., van Holstein, R. G., et al. 2020, *A&A*, 633, A63
 De Rosa, R. J., Nielsen, E. L., Wahhaj, Z., et al. 2023, *A&A*, 672, A94
 Debes, J. H., Poteet, C. A., Jang-Condell, H., et al. 2017, *ApJ*, 835, 205
 Debes, J., Nealon, R., Alexander, R., et al. 2023, *ApJ*, 948, 36
 Dohlen, K., Langlois, M., Saisse, M., et al. 2008, *Proc. SPIE*, 7014, 70143L
 Dong, R., Zhu, Z., Rafikov, R. R., & Stone, J. M. 2015a, *ApJ*, 809, L5
 Dong, R., Hall, C., Rice, K., & Chiang, E. 2015b, *ApJ*, 812, L32
 Dong, R., Zhu, Z., Fung, J., et al. 2016a, *ApJ*, 816, L12
 Dong, R., Fung, J., & Chiang, E. 2016b, *ApJ*, 826, 75
 Dong, R., Najita, J. R., & Brittain, S. 2018, *ApJ*, 862, 103
 Follette, K. B., Close, L. M., Males, J. R., et al. 2023, *AJ*, 165, 225
 Franson, K., Bowler, B. P., Zhou, Y., et al. 2023, *ApJ*, 950, L19
 Gaia Collaboration (Vallenari, A., et al.) 2023, *A&A*, 674, A1
 Garufi, A., Benisty, M., Pinilla, P., et al. 2018, *A&A*, 620, A94
 Haffert, S. Y., Bohn, A. J., de Boer, J., et al. 2019, *Nat. Astron.*, 3, 749
 Keppler, M., Benisty, M., Müller, A., et al. 2018, *A&A*, 617, A44
 Kharchenko, N. V. 2001, *Kinematika i Fizika Nebesnykh Tel*, 17, 409
 Kraus, S., Kreplin, A., Fukugawa, M., et al. 2017, *ApJ*, 848, L11
 Lagrange, A. M., Meunier, N., Rubini, P., et al. 2019, *Nat. Astron.*, 3, 1135
 Long, F., Andrews, S. M., Zhang, S., et al. 2022, *ApJ*, 937, L1
 Macintosh, B., Graham, J. R., Barman, T., et al. 2015, *Science*, 350, 64
 Maire, A.-L., Langlois, M., Dohlen, K., et al. 2016, *Proc. SPIE*, 9908, 990834
 Maire, A. L., Langlois, M., Delorme, P., et al. 2021, in *SF2A-2021: Proceedings of the Annual meeting of the French Society of Astronomy and Astrophysics*, ed. A. Siebert, 129
 Mesa, D., Gratton, R., Kervella, P., et al. 2023, *A&A*, 672, A93
 Monnier, J. D., Harries, T. J., Bae, J., et al. 2019, *ApJ*, 872, 122
 Montesinos, M., & Cuello, N. 2018, *MNRAS*, 475, L35
 Nielsen, E. L., De Rosa, R. J., Wang, J. J., et al. 2020, *AJ*, 159, 71
 Nowak, M., Lacour, S., Lagrange, A. M., et al. 2020, *A&A*, 642, L2
 Ohta, Y., Fukagawa, M., Sitko, M. L., et al. 2016, *PASJ*, 68, 53
 Ren, B., Dong, R., Esposito, T. M., et al. 2018, *ApJ*, 857, L9
 Ren, B., Dong, R., van Holstein, R. G., et al. 2020, *ApJ*, 898, L38
 Ren, B. B., Benisty, M., Ginski, C., et al. 2023, *A&A*, in press, <https://doi.org/10.1051/0004-6361/202347353>
 Safonov, B. S., Strakhov, I. A., Goliguzova, M. V., & Voziakova, O. V. 2022, *AJ*, 163, 31
 Schmid, H. M., Bazzon, A., Roelfsema, R., et al. 2018, *A&A*, 619, A9
 Shuai, L., Ren, B. B., Dong, R., et al. 2022, *ApJS*, 263, 31
 Spiegel, D. S., & Burrows, A. 2012, *ApJ*, 745, 174
 Stolker, T., Bonse, M. J., Quanz, S. P., et al. 2019, *A&A*, 621, A59
 van Holstein, R. G., Snik, F., Girard, J. H., et al. 2017, *Proc. SPIE*, 10400, 1040015
 van Holstein, R. G., Girard, J. H., de Boer, J., et al. 2020, *A&A*, 633, A64
 Vieira, S. L. A., Corradi, W. J. B., Alencar, S. H. P., et al. 2003, *AJ*, 126, 2971
 Vigan, A., Fontanive, C., Meyer, M., et al. 2021, *A&A*, 651, A72
 Wagner, K., Stone, J. M., Spalding, E., et al. 2019, *ApJ*, 882, 20
 Wagner, K., Stone, J., Skemer, A., et al. 2023, *Nat. Astron.*, 7, 1208
 Wallack, N. L., Ruffio, J. B., Ruane, G., et al. 2023, *AJ*, in press
 Wang, J. J., Ginzburg, S., Ren, B., et al. 2020, *AJ*, 159, 263
 Willson, M., Kraus, S., Kluska, J., et al. 2019, *A&A*, 621, A7
 Wölfer, L., Facchini, S., van der Marel, N., et al. 2023, *A&A*, 670, A154
 Xie, C., Ren, B., Dong, R., et al. 2021, *ApJ*, 906, L9
 Xie, C., Ren, B. B., Dong, R., et al. 2023, *A&A*, 675, L1
 Yu, S.-Y., Ho, L. C., & Zhu, Z. 2019, *ApJ*, 877, 100
 Zhang, S., Zhu, Z., Huang, J., et al. 2018, *ApJ*, 869, L47
 Zurlo, A., Vigan, A., Mesa, D., et al. 2014, *A&A*, 572, A85

Appendix A: Alternative measurements

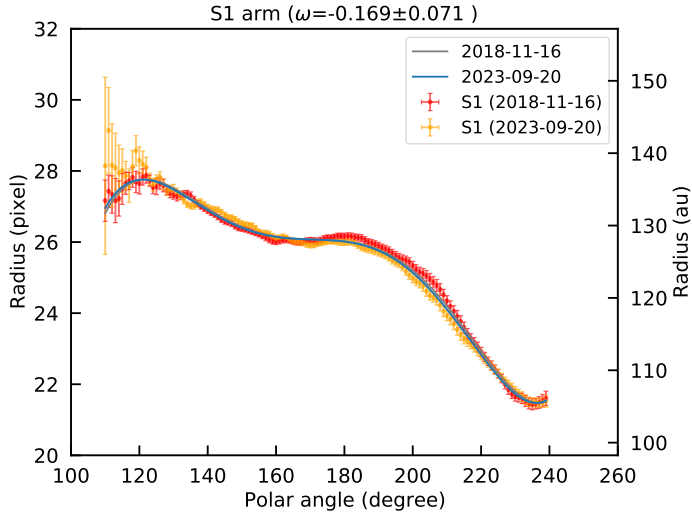


Fig. A.1. Peak locations of spiral arm S1 (full arm) in polar coordinates after correction for viewing geometry. The solid curves represent the best-fit model spiral for the peak locations (dots) between 2018 and 2023 ($t = 4.84$ yr), assuming the companion-driven scenario. The derived angular velocities of the motion of the spiral pattern are $-0^{\circ}.17 \pm 0^{\circ}.07 \text{ yr}^{-1}$.

We present the measured values for the entirety of the S1 and S2 arms here. The $\approx 30^{\circ}$ inclination effects (Dong et al. 2016b) and

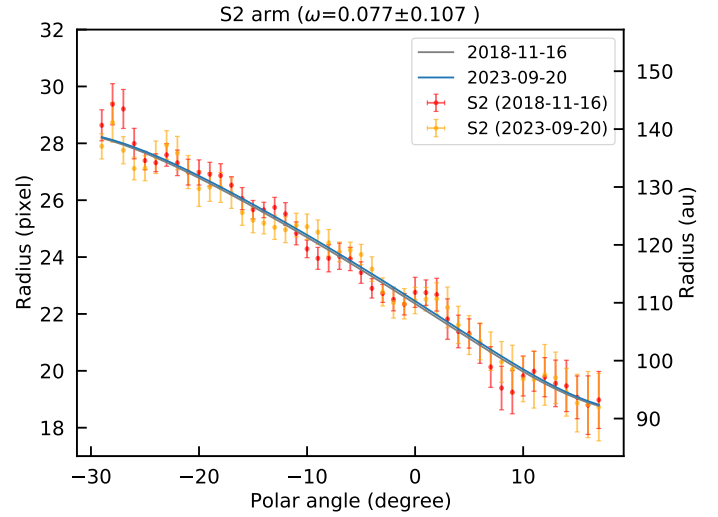


Fig. A.2. Peak locations of spiral arm S2 in polar coordinates after correction for viewing geometry. The solid curves represent the best-fit model spiral for the peak locations (dots) between 2018 and 2023 ($t = 4.84$ yr), assuming the companion-driven scenario. The derived angular velocities of the motion of the spiral pattern are $0^{\circ}.08 \pm 0^{\circ}.10 \text{ yr}^{-1}$.

shadowing effects (Montesinos & Cuello 2018) in Fig. 1 bias the motion of the entire spirals. However, we present the results here to show the global motion, which might be indicative of eccentric drivers (Calcino et al. 2020; Xie et al. 2023).